PCCP

ROYAL SOCIETY OF CHEMISTRY

PAPER

View Article Online
View Journal | View Issue





Cite this: *Phys. Chem. Chem. Phys.*, 2020, **22**, 22609

# The effect of elevated temperatures on excitonic emission and degradation processes of $WS_2$ monolayers

Reelika Kaupmees, *[a] Peter Walke,[a] Lukas Madauß, [b] Andre Maas,[b] Erik Pollmann, [b] Marika Schleberger, [b] Maarja Grossberg[a] and Jüri Krustok[ac]

Received 17th June 2020,
Accepted 21st September 2020

DOI: 10.1039/d0cp03248d

rsc.li/pccp

Controlled heating experiments in an inert environment have been performed on $WS_2$ monolayers, in order to clarify the conflicting reports on the high-temperature photoluminescent response of 2D TMDs. We find that in contrast to some previous results on both $WS_2$ and $MoS_2$, the photoluminescent intensity shows a consistent reduction above room temperature. This is accompanied by an almost linear redshift of the peak maximum, and a nearly linear increase in the peak width, which is attributed to an enhanced interaction with optical phonons. Moreover, by fitting the photoluminescence integral intensity with an Arrhenius type dependence, we demonstrate that the center of the $WS_2$ monolayer flake starts to undergo irreversible degradation at a temperature of 573 K in an inert environment. Regions close to flake edges in contrast, with a more intense room temperature PL response, remain stable. The macroscopic PL signal is largely recovered in these regions following subsequent cooling to room temperature.

## Introduction

Two-dimensional (2D) transition metal dichalcogenides (TMDs) have many interesting properties for future flexible optoelectronic and electronic applications.[1,2] These include, but are not limited to, field-effect transistor sensors,[3] field-effect transistors,[4] valleytronic based devices[5] and photodetectors[6] with the potential for significant performance improvements over the current state of the art. Moreover, specific properties can be tuned by changing the structure, phase or layer-number, whilst phases with mixed stoichiometry and vertical or horizontal heterostructures with other TMDs or 2D materials can all be combined to deliver optimal performance depending on the specific application requirements.

Of the wide variety of TMDs, monolayered $WS_2$ is particularly promising for many optoelectronic applications as it exhibits the largest direct band-gap[7] and typically the most intense photoluminescence (PL) response.[8] The room temperature PL spectrum of $WS_2$ is dominated by the so-called A exciton peak, arising from transitions between the lowest conduction and highest valence bands. The peak position of the A exciton of mechanically exfoliated $WS_2$ monolayers is found to be at around 2.0 eV.[9] However, the specific position is very sensitive to preparation method and substrate properties. In the case of chemical vapor deposition (CVD) grown $WS_2$ monolayers on $Si/SiO_2$, the built-in strain and altered charge-carrier concentration causes the exciton PL peak to redshift.[10,11] In turn, this strain will usually be relaxed when such monolayers are transferred to another substrate.[12] PL emission intensity is also affected by the defects in monolayers. Their precise influence is complex, and two types of defects, radiative and non-radiative, have been proposed.[13] The radiative defects seem to be concentrated at the edges and at grain boundaries.[14]

An interesting feature of $WS_2$ and other TMDs is the exceptionally high exciton binding energy,[15] thus making excitonic emission observable at high temperatures. Indeed, Li *et al.*[16] have proposed that $MoS_2$ monolayers can be used in opto-electronics devices with elevated working temperature. However, a variety of contrasting phenomena have so far been observed through high temperature PL experiments of the A exciton peak. For example, an increase in PL intensity with temperature,[16,17] an increase followed by a subsequent decrease,[16] or a monotonic decrease with increasing temperature,[18] have all been previously reported from temperature dependent PL measurements on monolayer $MoS_2$.

Other systems have similarly shown contradictory behavior. PL enhancement at temperatures above 300 K has been observed also in few-layer $WSe_2$[19] and in multi-layered $WS_2$,[20] whilst Chen *et al.*[17] also reported a transient high temperature

[a] *Department of Materials and Environmental Technology, Tallinn University of Technology, Ehitajate tee 5, 19086 Tallinn, Estonia. E-mail: reelika.kaupmees@taltech.ee*
[b] *Faculty of Physics and CENIDE, University of Duisburg-Essen, Lotharstr. 1, Duisburg 47057, Germany*
[c] *Division of Physics, Tallinn University of Technology, Ehitajate tee 5, 19086 Tallinn, Estonia*

increase of PL intensity in single-layer $WS_2$ following an initial decrease above room temperature, although this was then followed again by a subsequent decrease with further increase in temperature. These results are unusual given the typical reduction of PL intensity of semiconductors at elevated temperatures. In contrast Gaur *et al.*[21] have shown a decrease in PL intensity at all stages of temperature increase from 83–473 K for $WS_2$ flakes grown on sapphire. Similar behavior was also seen by Su *et al.*,[22] who noted a red-shift in peak position and decrease in intensity for both an irregularly shaped film grown on $Si/SiO_2$ and a monolayer grown on sapphire. Finally, the integrated PL intensity has been observed to decrease in vertically stacked $WS_2/MoS_2$ monolayer heterostructures at temperatures above room temperature due to the thermally activated non-radiative recombination mechanism.[23]

Furthermore, high temperature measurements are also necessary for establishing operating conditions in future applications, many of which will practically involve elevated working temperatures, as well as quantifying changes to photophysical parameters beyond intensity that may be incurred in such situations. Moreover, degradation of TMDs has been seen at high temperatures. In monolayered $MoS_2$, small triangular holes appear in systems subjected to a hydrogen and argon mixed atmosphere at around 773 K[24] and grain boundary degradation has been seen when heated in air.[25] Still, while the PL properties of $WS_2$ monolayers at low temperatures have been studied extensively in multiple papers such as ref. 11 and 26, there are only a few studies about high temperature PL measurements and even less information about degradation of flakes at elevated temperatures and in different atmospheres. Taken with the conflicting accounts of the temperature-dependent photoluminescent response of TMD monolayers, this points to a need for further clarification, both to provide greater mechanistic insights and to establish maximal device operating conditions.

Herein, we focus on the properties of $WS_2$ monolayers using PL measurements at elevated temperatures, and how these temperatures consequently affect the degradation of the flakes. We clarify the high-temperature photoluminescent response of the monolayer, and detail the induced irreversible changes upon return to room temperature. Our work shall serve as a basis for further fundamental and applied studies on 2D TMDs at high temperatures.

## Experimental

### CVD growth

$WS_2$ monolayers were fabricated using a multi-zone split tube furnace with thermally separated heating zones (ThermConcept, ROK 70/750/12-3z). The substrates were $Si/SiO_2$ wafers. First, ammonium tungsten oxide hydrate (ATH) was dissolved in deionized water. The solution with 1000 g $l^{-1}$ was transferred onto a first substrate in several little droplets of $\sim$1 mm in diameter. Subsequently, the substrate was heated under ambient atmosphere at 500 °C for 30 min to convert ATH into the tungsten source $WO_3$. Afterwards, cholic acid sodium salt (CAS) was spin coated as the seeding promoter onto the substrate containing $WO_3$ as well as onto a second otherwise clean substrate. The substrate with $WO_3$ was put into a crucible, the second substrate – only with seeding promoter – was flipped and put upside down onto the first one. The crucible containing the substrate and the tungsten source was put into the center heating zone and a second crucible filled up with 100 mg sulfur was put into the heating zone upstream. After sealing, the tube was purged with Ar gas. For the CVD process the Ar flow rate was set to 50 sccm. The central heating zone was heated to 825 °C in 20 min and the sulfur heating zone to 150 °C in 10 min after a delay of 10 min. After holding the maximum temperatures for 30 min, the furnace was opened for rapid cooling.

### Characterization

Raman, reflectance contrast (RC) and μ-PL measurements were carried out using a Horiba LabRAM HR800 Micro-Raman system equipped with a multichannel CCD detection system in the backscattering configuration with a spectral resolution better than 1 $cm^{-1}$. A continuous wave Nd-YAG laser (wavelength 532 nm) was used for excitation. Excitation powers used in the study were 0.03–0.42 mW. Two different objectives were used for measurements: a 10× long-working-distance lens (NA = 0.25) with bigger laser spot size (approximately marked as area 1 in Fig. 3(a)) and a 50× long-working-distance lens (NA = 0.50) with smaller laser spot size (approximately marked as area 2 in Fig. 3(a)). The used laser beam was linearly polarized and therefore the sample orientation was kept constant during the temperature dependent PL measurements. A Linkam THMS600 heating/cooling stage was used for temperature dependent PL measurements ($T$ = 298–723 K). Before measurements, the cryostat was flushed with Ar gas for approximately 10 minutes and after that the valves were closed. The pressure at room temperature was around 2 atm. While the sample was heated, the cryostat housing had a water-cooling system. Samples were heated with a 10 K $min^{-1}$ rate and were held at desired temperatures for a least 5 min to let the sample temperature to stabilize. Measurements were performed in an argon atmosphere, preventing $WS_2$ flakes from oxidizing. An atomic force microscope (AFM; Bruker Multimode) with a Nanoscope V controller was used to determine the thickness of the layers. PL imaging was carried out on a microscope unit with a high-power 420 nm light emitting diode (Thorlabs M420L3) for wide-field excitation and for detection through a 50× objective a cooled Atik 414EX CCD camera (filters to remove excitation emission were employed).

## Results and discussion

CVD grown $WS_2$ monolayers exhibited a variety of different shapes with the average domain size around 100 μm. An atomic force microscope was used to determine the thickness of the monolayers, which was found to be about 0.8 nm (Fig. 1(a and b)), a typical value for TMD monolayers.[21] This finding was supported by initial optical characterization by Raman spectroscopy. A Raman spectrum was measured from the area 2, in Fig. 3(a) and the results are presented in Fig. 1(c). From the Raman fitting the

 

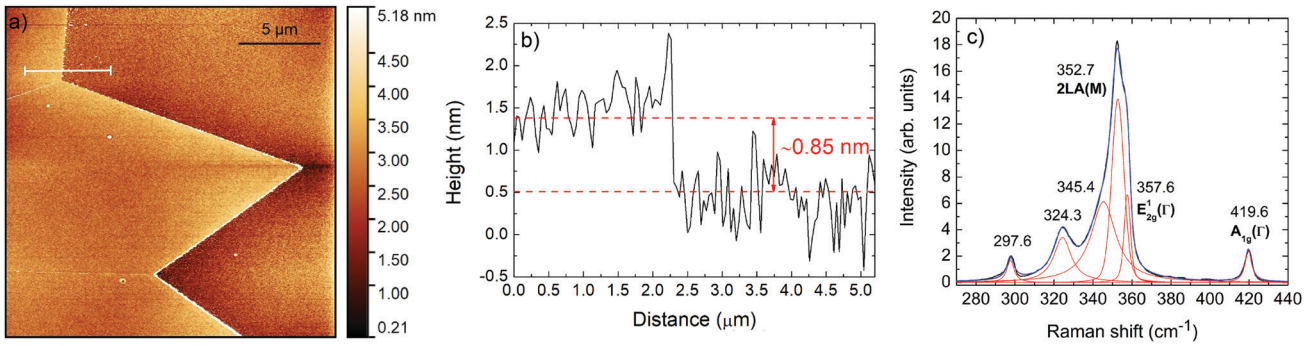


Fig. 1 AFM height image (a) and AFM line profile (b) showing typical $WS_2$ monolayer thickness. The line profile was taken along the white line shown in (a). Raman spectrum (c) from the $WS_2$ monolayer. Red lines show the result of spectral fitting using Lorentzian curves.

peak positions of the main peaks, the in-plane mode $E^1_{2g}(\Gamma)$ at 357.6 cm$^{-1}$ and the out-of-plane mode $A_{1g}(\Gamma)$ at 419.6 cm$^{-1}$ were determined. The separation of these peaks is $\Delta$ = 62.0 cm$^{-1}$, which is in the same range ($\Delta$ = 61.5–62.4 cm$^{-1}$) previously found in good quality $WS_2$ monolayers.[8,27–29] Additionally, a strong peak assigned to a second-order contribution (2LA(M)) was also seen at 352.7 cm$^{-1}$, as is typical for measurements on $WS_2$ monolayers under near-resonance conditions.[29]

Fig. 2(b) shows a PL image of a $WS_2$ polycrystalline monolayer flake and Fig. 2(b) shows a PL image of the same flake after it was heated in an Ar atmosphere up to $T$ = 643 K, detailing the formation of cracks along the grain boundaries. $WS_2$ flakes started to be thermally unstable at around $T$ = 573 K as was seen in the optical microscope. One reason for this cracking could be the different thermal expansion of the substrate and the $WS_2$ monolayer.[12] Although this should not play such a big role, because the CVD growth temperature is $T$ = 1073 K and the material can handle temperature difference between growth and room temperatures, so the stress at $T$ = 573 K should not have such an effect. However, defects at grain boundaries can affect the material loss. This phenomenon has been seen also in $MoS_2$ monolayers heated in air.[25]

As shown in Fig. 2(a) grain boundaries and their degradation at higher temperature can have a crucial influence on the PL emission. For further PL studies an equilateral triangular shaped $WS_2$ flake was chosen. This type of flake is monocrystalline and without visible grain boundaries, unlike other shapes, in which original monocrystalline flakes have ripened into a larger irregular structure with internal grain boundaries.[30] The following PL temperature dependence study was carried out with a 10× objective (NA = 0.25), so the laser spot would cover a maximum area and thus the spatial variations in the flake are averaged with the surrounding region (see area 1 in Fig. 3(a)). To study the PL response of the area where the monolayer is still intact after the temperature dependence study (Fig. 3(b)) a 50× objective (NA = 0.50) was used (see area 2). The initial room temperature PL image in Fig. 3(a) shows that the PL intensity across the monolayer is non uniform. As has been previously reported, the center of the crystal shows lower PL intensity than the areas close to the edges,[13] with this region of lower intensity also extending symmetrically from the center towards the vertices.

The temperature dependence of some PL spectra is presented in Fig. 4(a). All temperature dependent PL spectra had an asymmetrical shape and were fitted using Split Pearson VII function,[31] with the fittings also shown in Fig. 4(a). The laser power used for temperature dependent measurements ($T$ = 303–723 K) was 0.42 mW. Although the asymmetrical A exciton peak can be observed in the whole temperature range, with increasing temperature the peak intensity was seen to decrease in contrast to ref. 16 and 17, whilst the peak position was seen to red-shift and the FWHM to broaden. The temperature dependence of the A exciton peak position is linear with $dE_{max}/dT = -0.358 \pm 0.003$ meV K$^{-1}$ (Fig. 4(b)).

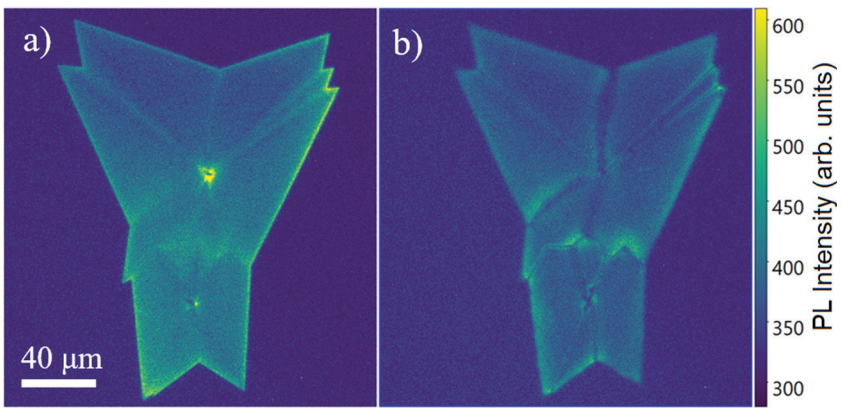


Fig. 2 PL images of the same flake before (a) and after (b) heating the sample up to $T$ = 643 K. Cracking can be observed at the grain boundaries.

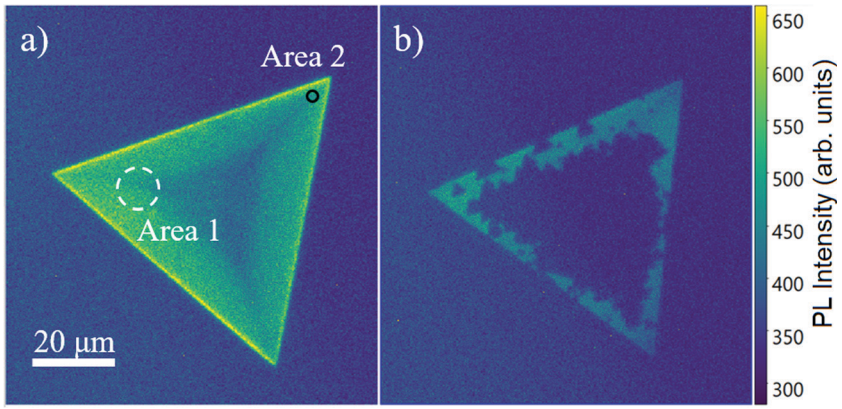


Fig. 3 PL images of the same flake before (a) and after (b) it was used to study temperature dependent PL at elevated temperatures. Area 1 and area 2 are representing the approximate laser spot size and placement of 10× objective and 50× objective, respectively.

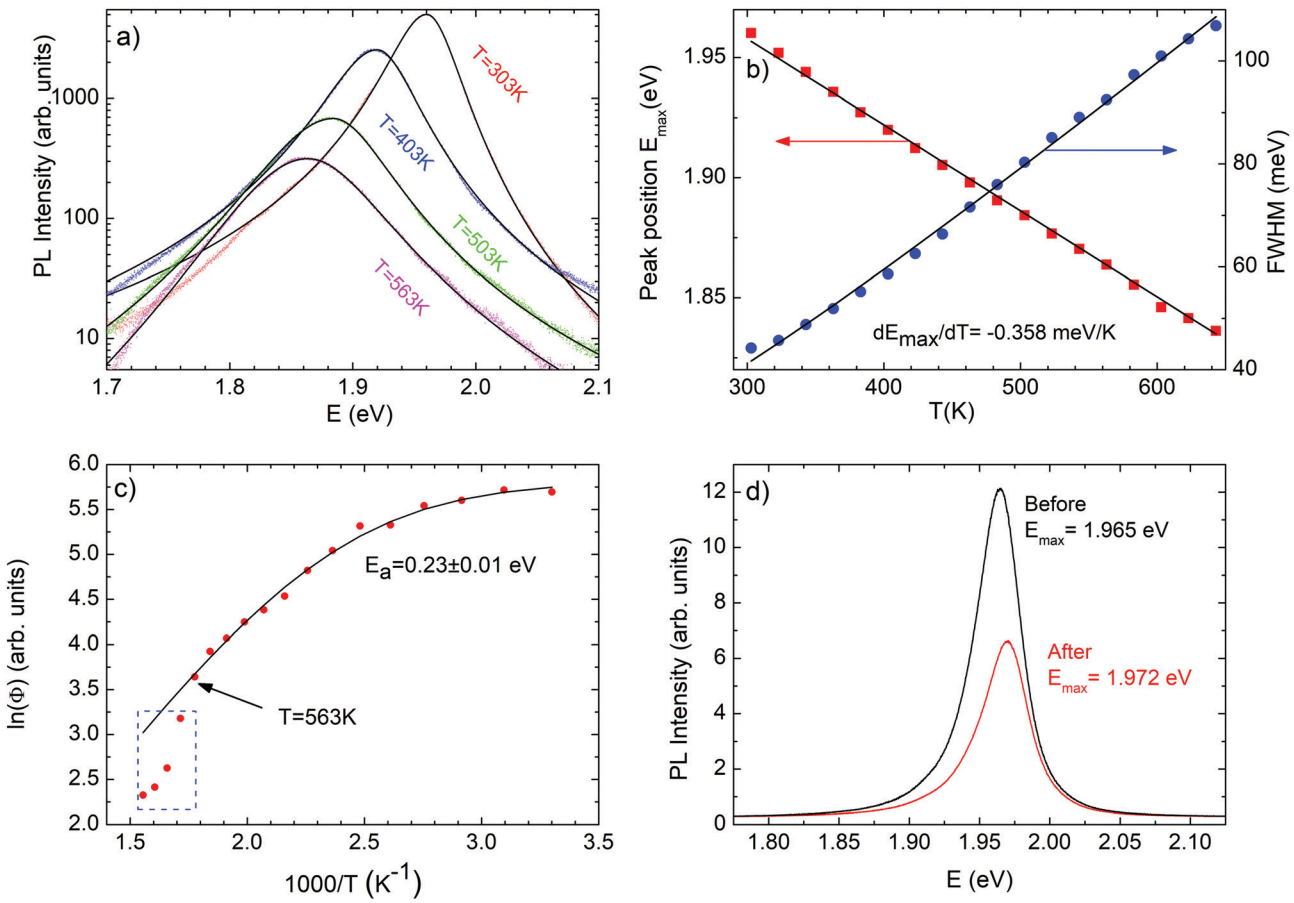


Fig. 4 (a) Temperature dependent PL spectra of $WS_2$ monolayer. PL fitting using Split-Pearson-VII function are shown as black lines. (b) Temperature dependence of exciton peak energy (red dots) and FWHM of the exciton peak (blue dots). The exciton peak energy dependence is fitted with linear and FWHM dependence is a result of fitting with eqn (1). (c) Arrhenius style plot showing the thermal activation energy of the A exciton peak. Fitting result using eqn (2) is given as a continuous line. Blue rectangle is showing the additional intensity decrease due to material decomposition. (d) Room temperature PL spectra form area 2 of Fig. 3(a) on the flake before and after heating up to $T$ = 723 K.

Next, the temperature dependence of the full-width at half-maximum (FWHM) was fitted using the relation proposed by Rudin *et al.*[32] given as

$$\mathrm{FWHM}(T) = W_0 + \beta T + \gamma/[\exp(\hbar\omega_{\mathrm{LO}}/kT) - 1] \quad (1)$$

where $W_0$ is the width at $T = 0$ K including also inhomogeneous broadening, $\beta$ is a coefficient for the interaction of excitons with acoustic phonons and the last term represents the interaction with LO (longitudinal optical) phonons, $\hbar\omega_{\mathrm{LO}}$ is the LO-phonon energy and is taken to be equal to 44.6 meV for $WS_2$.[33]

 

The interaction with acoustic phonons was neglected because it is usually very small.[34] The fitting result is presented in Fig. 4(b) and fitting parameters are the following $W_0$ = 16.5 ± 0.8 meV and $\gamma$ = 113.9 ± 1.6 meV. The FWHM of the exciton peak increases in the whole temperature range due to interaction with LO phonons.

Subsequently, the thermal activation energy of $WS_2$ exciton emission was found to be $E_a$ = 0.23 ± 0.01 eV (Fig. 4(c)), as was determined using the following equation:[35]

$$\Phi(T) = \Phi_0 \Big/ \left(1 + a e^{-\frac{E_a}{kT}}\right) \quad (2)$$

where $\Phi$ is the integral intensity of the PL band, $a$ is the process rate parameter and $E_a$ is the thermal activation energy. Thermal quenching of exciton emission is probably related to activation of non-radiative recombination.[22,36] For the calculation of the thermal activation energy temperatures up to $T$ = 563 K were involved, because when the temperature was higher than $T$ = 563 K we noticed an additional drop of PL intensity due to decomposition of the $WS_2$ monolayer (marked with the blue rectangle in Fig. 4(c)). Similar activation energies have been found in $WS_2$ grown on $Si/SiO_2$ ($E_a$ = 0.40 eV[22] and $E_a$ = 0.53 eV[36]) and on sapphire ($E_a$ = 0.20 eV).[22]

Room temperature PL was measured before and after heating (up to $T$ = 723 K) from area 2 (see Fig. 3(a)), a region that had not undergone apparent thermal decomposition. The results are presented in Fig. 4(d). The PL intensity at room temperature following the high temperature measurements remained in a similar range as before although the intensity has reduced by about a factor of two. This indicates that the remaining $WS_2$ monolayer is stable against temperature variations and largely maintains its previous properties, suggesting that the temperature does not have some irreversible effect on the monolayer that remains. The Raman spectrum from the same area after heating up to $T$ = 723 K shows a peak separation of $\Delta$ = 61.9 $cm^{-1}$ and the shape of the spectrum remained the same, confirming that the quality of remaining monolayer is maintained. Additionally, reflectance contrast measurements can be also used to further study the quality of $WS_2$ monolayer. It is known that the absorption spectrum is directly related to the reflectance contrast spectrum:[37]

$$\frac{\Delta R}{R}(E) = \frac{R_L - R_S}{R_S} = \frac{4}{n_S^2 - 1}\alpha(E) \quad (3)$$

where $R_L$ is a reflected light from the monolayer, $R_S$ is a reflected light from the $SiO_2$ substrate layer, $n_s$ is the index of refraction of the $SiO_2$ layer and $\alpha$ is the absorption of the sample. RC spectra measured before and after heating ($T$ = 723 K) are presented in Fig. 5. It can be seen that the shape and intensity of A and B exciton bands remain relatively unchanged after thermal treatment.

From Fig. 3(b) it seems that the remaining $WS_2$ monolayer is concentrated near the edges of a triangle. It is also interesting to note that this part of the flake exhibited a greater room temperature PL intensity compared to the central part of the monolayer. This means that the central part of the triangle, that has lower PL intensity, is also degrading faster at high temperatures than the brighter part of the flake. It may be that

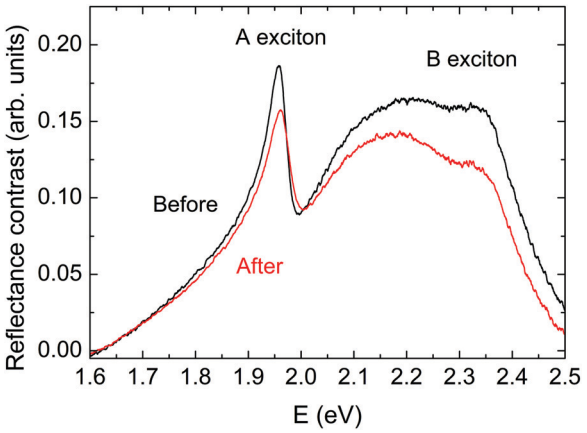


Fig. 5 Room temperature RC spectra form $WS_2$ flake before and after heating up to $T$ = 723 K.

the middle area of the triangle has more defects, which are non-radiative[13] and that this is the reason for material loss. Moreover, our measurements showed that the PL band from the middle area of the as-grown flake was also red shifted about 4 meV when compared to the edge region of the flake. This red shift of the exciton band in CVD grown monolayers is related to the slightly higher value of tensile strain.[10,26] It is possible that the increased strain is also playing an essential role in more rapid thermal decomposition of the central part of the flake. This is further corroborated by the polycrystalline flake (Fig. 2), which has the most significant material loss starting at the grain boundaries, although this flake was exposed to even lower temperatures ($T$ = 643 K). However, the remaining monolayer does also include some areas of material loss that also exhibit a triangular shape. These triangular holes are probably related to point defects. The intrinsic defects in as-grown $MoS_2$, including grain boundaries and point defects, as starting points for degradation are discussed also in ref. 38. Specifically, areas with higher defect density have larger concentrations of dangling bonds and consequently greater reactivity. Moreover, the authors noticed that triangular holes due to point defects have opposite orientation to the parent crystal. This can also be observed in our case (see Fig. 3(b)). The PL peak position after high temperature handling had a small blue-shift of 7 meV, which may be related to strain release,[10] as the material loss and geometry change of the flake can affect the strain inside the flake. The same small blue-shift of the A-exciton can be observed also in the RC spectrum after high-temperature handling, see Fig. 5.

It is also noteworthy that whilst the first apparent material loss was detected in the optical image at $T$ = 603 K, it is evident from the spectroscopy data that initial degradation begins at around $T$ = 563 K. The intensive material loss after high temperature treatment is visible in Fig. 3(b), in which only some areas of the original triangle are still present.

AFM was used to further study the intact monolayer, with the results presented in Fig. 6. The height and phase scans (Fig. 6(a and b) respectively) show that the holes inside the material are indeed of triangular shape. Furthermore, the inside of the triangle (right side of the Fig. 6(a)) includes areas with

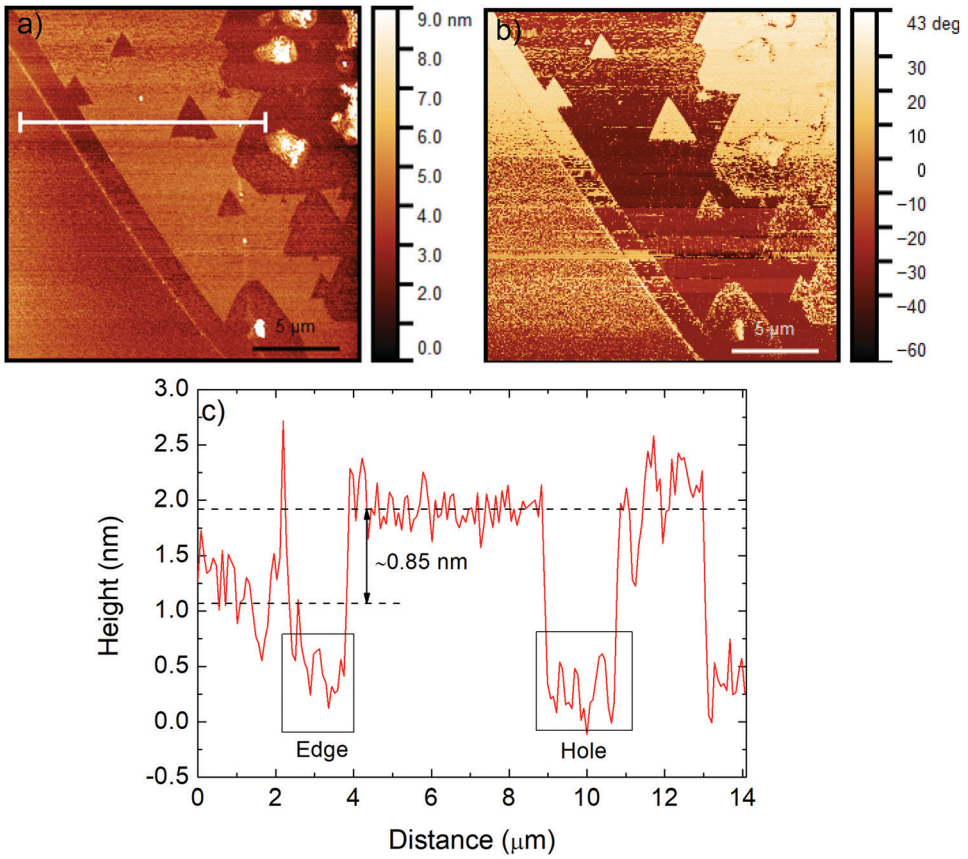


Fig. 6 AFM height (a) and phase (b) image of the studied flake edge after high temperature measurements up to $T$ = 723 K. Line profile (c) is presented in red color (white line from Fig. 6(a)).

large aggregations of material. According to the phase image, these regions are not crystalline $WS_2$, a finding that is further confirmed by Fig. 3(b), as these regions are not seen to emit PL. As such, they may be collections of amorphous material, which consist of decomposed $WS_2$ monolayer remnants.

A second change that can be observed from the AFM results is that the $WS_2$ monolayer edge has been shifted, whilst there is also a very thin line marking the former edge visible in Fig. 6. Although this shift of the edge is only by about 1 μm, it is still noticeable in Fig. 3, where the size of the triangle is smaller after high temperature measurements. The treatment also seems to have had some effect on the underlying substrate ($SiO_2$), as evidenced from the black rectangle marked edge in Fig. 6(c). Here, part of the underlying $SiO_2$ between the original and new $WS_2$ appears to have been eroded. Although we note that an imaging artifact cannot be ruled out, this apparent substrate degradation is also present in the eroded regions within the remaining monolayer (black rectangle marked as hole in Fig. 6(c)). In turn, one possible reason for the shift of the edge may be due to a higher concentration of defects on the edge, as was discussed previously. The intrinsic defects can be located in grain boundaries or at edges, or be present as local point defects and are the starting point for the degradation.

As stated earlier, contradictory reports can also be found regarding the high-temperature photoluminescent response of other TMDs, such as $MoS_2$. Many of the monolayered TMD materials (including $MoS_2$) have similar structures and properties to $WS_2$, and similar general trends to those found here could be tentatively expected in such cases. However, we note that the individual materials are distinct, and it is difficult to predict with certainty the behavior of these other systems without further measurements.

## Conclusion

In this report we have detailed the changes in the excitonic emission of monolayer $WS_2$ induced by high temperature, as well as described the degradation induced and the extent of recovery upon a return to room temperature. Rather than seeing a transient or consistent enhancement in PL intensity upon raising the temperature, our measurements in a controlled environment show a standard and continuous decrease in intensity. This is allied to a near linear decrease in peak position and to an increase in peak width, and is considered to result from exciton interaction with optical phonons.

We also note degradation of parts of the monolayer following the handling at elevated temperatures, whilst other parts largely maintain their original properties, such as position and shape of Raman peaks and PL intensity. The irreversible changes at high

 

temperature were first established by an additional reduction in PL intensity prior to any changes being visible in the appearance of the monolayer. Moreover, there is an apparent relation between the areas of lower initial room temperature PL intensity in the center of the flake and the degree of material loss from the monolayer. Additionally, the symmetry of the holes detected in the remaining monolayer by AFM may point to a defect induced mechanism, suggesting that a higher density of defects in the flake center may be responsible for both the weaker PL intensity and enhanced rate of degradation. However, this paints an incomplete picture given the additional loss of material from the very edge of the flake, which shows very high relative PL intensity at room temperature. Hence, further investigations are needed to deepen the understanding of temperature-induced degradation mechanisms. Beyond this, our work can also be extended to look at the role of other micro or macroscopic parameters, such as stoichiometry, flake shape, or substrate, on the high-temperature photo-response of 2D TMDs.

## Conflicts of interest

There are no conflicts to declare.

## Acknowledgements

This work has been supported by the European Regional Development Fund, Project TK141. L. M., A. M., E. P., and M. S. gratefully acknowledge support from DFG by funding SCHL 384/20-1 (project number 406129719).

## References

1 W. Choi, N. Choudhary, G. H. Han, J. Park, D. Akinwande and Y. H. Lee, *Mater. Today*, 2017, **20**, 116–130.
2 D. Akinwande, N. Petrone and J. Hone, *Nat. Commun.*, 2014, **5**, 5678.
3 H. Li, Z. Yin, Q. He, H. Li, X. Huang, G. Lu, D. W. H. Fam, A. I. Y. Tok, Q. Zhang and H. Zhang, *Small*, 2012, **8**, 63–67.
4 G. H. Lee, Y. J. Yu, X. Cui, N. Petrone, C. H. Lee, M. S. Choi, D. Y. Lee, C. Lee, W. J. Yoo, K. Watanabe, T. Taniguchi, C. Nuckolls, P. Kim and J. Hone, *ACS Nano*, 2013, **7**, 7931–7936.
5 Y. Liu, Y. Gao, S. Zhang, J. He, J. Yu and Z. Liu, *Nano Res.*, 2019, **12**, 2695–2711.
6 H. Wang, C. Zhang, W. Chan, S. Tiwari and F. Rana, *Nat. Commun.*, 2015, **6**, 6–11.
7 J. Gusakova, X. Wang, L. L. Shiau, A. Krivosheeva, V. Shaposhnikov, V. Borisenko, V. Gusakov and B. K. Tay, *Phys. Status Solidi*, 2017, **214**, 1700218.
8 H. R. Gutiérrez, N. Perea-López, A. L. Elías, A. Berkdemir, B. Wang, R. Lv, F. López-Urías, V. H. Crespi, H. Terrones and M. Terrones, *Nano Lett.*, 2013, **13**, 3447–3454.
9 I. Paradisanos, N. Pliatsikas, P. Patsalas, C. Fotakis, E. Kymakis, G. Kioseoglou and E. Stratakis, *Nanoscale*, 2016, **8**, 16197–16203.
10 Y. Wang, C. Cong, W. Yang, J. Shang, N. Peimyoo, Y. Chen, J. Kang, J. Wang, W. Huang and T. Yu, *Nano Res.*, 2015, **8**, 2562–2572.
11 J. Krustok, R. Kaupmees, R. Jaaniso, V. Kiisk, I. Sildos, B. Li and Y. Gong, *AIP Adv.*, 2017, **7**, 065005.
12 K. M. McCreary, A. T. Hanbicki, S. Singh, R. K. Kawakami, G. G. Jernigan, M. Ishigami, A. Ng, T. H. Brintlinger, R. M. Stroud and B. T. Jonker, *Sci. Rep.*, 2016, **6**, 1–10.
13 M. R. Rosenberger, H. J. Chuang, K. M. McCreary, C. H. Li and B. T. Jonker, *ACS Nano*, 2018, **12**, 1793–1800.
14 H. Liu, J. Lu, K. Ho, Z. Hu, Z. Dang, A. Carvalho, H. R. Tan, E. S. Tok and C. H. Sow, *Nano Lett.*, 2016, **16**, 5559–5567.
15 A. T. Hanbicki, M. Currie, G. Kioseoglou, A. L. Friedman and B. T. Jonker, *Solid State Commun.*, 2015, **203**, 16–20.
16 Y. Li, W. Liu, H. Xu, C. Zhang, L. Yang, W. Yue and Y. Liu, *J. Mater. Chem. C*, 2016, **4**, 9187–9196.
17 Y. Chen, W. Wen, Y. Zhu, N. Mao, Q. Feng, M. Zhang, H. P. Hsu, J. Zhang, Y. S. Huang and L. Xie, *Nanotechnology*, 2016, **27**, 445705.
18 P. J. Ko, A. Abderrahmane, T. V. Thu, D. Ortega, T. Takamura and A. Sandhu, *J. Nanosci. Nanotechnol.*, 2015, **15**, 6843–6846.
19 S. Zhu, D. Li, Y. Hu, J. Wang, X. Wang and W. Lu, *Mater. Res. Express*, 2018, **5**, 066209.
20 H. Chen, Y. Li, W. Liu, H. Xu, G. Yang, J. Shi, Q. Feng, T. Yu, X. Liu and Y. Liu, *Nanoscale Horiz.*, 2018, **3**, 598–605.
21 A. P. S. Gaur, S. Sahoo, J. F. Scott and R. S. Katiyar, *J. Phys. Chem. C*, 2015, **119**, 5146–5151.
22 L. Su, Y. Yu, L. Cao and Y. Zhang, *Nano Res.*, 2015, **8**, 2686–2697.
23 Z. Hu, Y. Bao, Z. Li, Y. Gong, R. Feng, Y. Xiao, X. Wu, Z. Zhang, X. Zhu, P. M. Ajayan and Z. Fang, *Sci. Bull.*, 2017, **62**, 16–21.
24 G. Ye, Y. Gong, J. Lin, B. Li, Y. He, S. T. Pantelides, W. Zhou, R. Vajtai and P. M. Ajayan, *Nano Lett.*, 2016, **16**, 1097–1103.
25 K. Yao, J. D. Femi-Oyetoro, S. Yao, Y. Jiang, L. El Bouanani, D. C. Jones, P. A. Ecton, U. Philipose, M. El Bouanani, B. Rout, A. Neogi and J. M. Perez, *2D Mater.*, 2020, **7**, 015024.
26 R. Kaupmees, M. Grossberg, M. Ney, A. Asaithambi, A. Lorke and J. Krustok, *Phys. Status Solidi RRL*, 2020, **14**, 1–6.
27 K. M. McCreary, A. T. Hanbicki, G. G. Jernigan, J. C. Culbertson and B. T. Jonker, *Sci. Rep.*, 2016, **6**, 19159.
28 Y. Zhang, Y. Zhang, Q. Ji, J. Ju, H. Yuan, J. Shi, T. Gao, D. Ma, M. Liu, Y. Chen, X. Song, H. Y. Hwang, Y. Cui and Z. Liu, *ACS Nano*, 2013, **7**, 8963–8971.
29 A. Berkdemir, H. R. Gutiérrez, A. R. Botello-Méndez, N. Perea-López, A. L. Elías, C. I. Chia, B. Wang, V. H. Crespi, F. López-Urías, J. C. Charlier, H. Terrones and M. Terrones, *Sci. Rep.*, 2013, **3**, 1–8.
30 E. Pollmann, L. Madauß, V. Zeuner and M. Schleberger, *Encyclopedia of Interfacial Chemistry: Surface Science and Electrochemistry*, 2018, **3**, 338–343.
31 D. Balzar, *J. Res. Natl. Inst. Stand. Technol.*, 1993, **98**, 321.
32 S. Rudin, T. L. Reinecke and B. Segall, *Phys. Rev. B: Condens. Matter Mater. Phys.*, 1990, **41**, 3017–3027.
33 A. Molina-Sánchez and L. Wirtz, *Phys. Rev. B: Condens. Matter Mater. Phys.*, 2011, **84**, 1–8.

34 S. Helmrich, R. Schneider, A. W. Achtstein, A. Arora, B. Herzog, S. M. de Vasconcellos, M. Kolarczik, O. Schöps, R. Bratschitsch, U. Woggon and N. Owschimikow, *2D Mater.*, 2018, **5**, 045007.
35 J. Krustok, H. Collan and K. Hjelt, *J. Appl. Phys.*, 1997, **81**, 1442–1445.
36 N. Peimyoo, J. Shang, C. Cong, X. Shen, X. Wu, E. K. L. Yeow and T. Yu, *ACS Nano*, 2013, **7**, 10985–10994.
37 K. F. Mak, M. Y. Sfeir, Y. Wu, C. H. Lui, J. A. Misewich and T. F. Heinz, *Phys. Rev. Lett.*, 2008, **101**, 196405.
38 X. Chen, S. M. Shinde, K. P. Dhakal, S. W. Lee, H. Kim, Z. Lee and J. H. Ahn, *NPG Asia Mater.*, 2018, **10**, 810–820.

 